Validity of bond-length and Mössbauer parameters to assign oxidation states in multicomponent oxides: Case study of $Sr_4Fe_4O_{11}$

P. Ravindran,* R. Vidya, H. Fjellvåg, and A. Kjekshus
Center for Materials Science and Nanotechnology, Department of Chemistry, University of Oslo, Box 1033 Blindern, N-0315 Oslo, Norway
(Received 23 January 2008; published 30 April 2008)

From analyses of structural information for oxides with Fe in different oxidation states and computationally estimated Mössbauer parameters (hyperfine field, isomer shift, and quadrupole splitting) based on density-functional theory, we show that the charges residing on the different constituents cannot be directly derived either from structural or Mössbauer measurements. We have analyzed charge density, charge transfer, electron localization function, crystal orbital Hamilton population, and partial density of states to explain the bonding characteristics. Born-effective charge tensor is used to quantify the charges present at the atomic sites in $Sr_4Fe_4O_{11}$. We show that the effects of covalence are important in explaining the electronic structure, magnetism, and chemical bonding in oxygen-vacancy-ordered systems such as $Sr_4Fe_4O_{11}$ and on ignoring covalence, one can be misled in oxidation-state assignments.

DOI: 10.1103/PhysRevB.77.134448 PACS number(s): 75.50.Ee

I. INTRODUCTION

The assignment of actual oxidation states to ions in mixed valent systems is a difficult task due to the uncertainties in establishing the total charge at different sites. Recently, based on the results from first-principles calculations, we have reported[1,2] that formal Fe^{3+} ions reside at the square-pyramidal sites and Fe^{4+} ions in the octahedral sites in mixed-valence oxygen-vacancy-ordered $Sr_4Fe_4O_{11}$. By comparing the experimentally measured structural and Mössbauer parameters for $Sr_4Fe_4O_{11}$ with those for reference systems, Adler[3] argued that Fe^{3+} and Fe^{4+} ions reside at the octahedral (o) and square-pyramidal (s) sites, respectively.

$Sr_4Fe_4O_{11}$ contains $Fe1^s$ and $Fe2^o$ ions in equal amounts, which occupy alternative positions in the lattice in an ordered manner. Hence, it has proven difficult to distinguish which of these sites antiferromagnetically (AF) order. Two detailed experimental reports are available on the assignment of the oxidation state to the Fe sites and the specification of the magnetic structure of $Sr_4Fe_4O_{11}$. However, the conclusions are contrary to each other. Hodges *et al.*[4] concluded that Fe1 and Fe2 take the 4+ and 3+ oxidation state, respectively, whereas Schmidt *et al.*[5] concluded oppositely. Likewise, Hodges *et al.*[4] concluded that the $Fe2^o$ moments exhibit long-range AF order whereas the $Fe1^s$ moments are magnetically frustrated, and Schmidt *et al.*[5] arrived at the opposite conclusion. The results from our theoretical calculations show that the $Fe1^s$ and $Fe2^o$ sites have 3+ and 4+ oxidation states, respectively, with the $Fe2^o$ moments AF ordered.

In this paper, we analyze the applicability of bond lengths to assign oxidation states not only in $Sr_4Fe_4O_{11}$ but also in various other Fe-containing oxides. We also present a detailed account of the bonding characteristics in $Sr_4Fe_4O_{11}$ by using various theoretical tools. In practice, the Mössbauer parameters such as hyperfine field, isomer shift, and quadrupole splitting are measured and compared to those of other compounds with unambiguous oxidation states. Hence, we have theoretically simulated these parameters for $Sr_4Fe_4O_{11}$ and compared them to other well known compounds. In addition, we present a very detailed analysis of the various factors influencing these parameters.

II. CORRELATION BETWEEN OXIDATION STATE AND Fe-O BOND LENGTH

The common conception behind a correlation between bond length and oxidation state is that ions with lower oxidation states should generally have larger ionic radii and consequently occupy a relatively larger volume in a crystal. However, the opposite is apparently true for Fe in oxides. For example, Ref. 7 lists the ionic radii of Fe in the oxidation states 2+ and 3+ as 1.734 and 1.759 Å, respectively. The $d_{Fe\text{-}O}$ for square-pyramidal (1.864 Å) coordination in $Sr_4Fe_4O_{11}$ fits well with that for 3+ ions in tetrahedral (1.875 Å) sites. On the contrary, the $Fe1^s$-O and $Fe2^o$-O bond lengths are longer than that for 4+ ions in tetrahedral and octahedral coordinations, respectively.

The experimentally derived average bond length for Fe ions in different oxidation states are given in Table I. From this compilation, it is seen that among the different valence states, Fe prefers to take the 3+ state in oxides. The formal Fe^{5+} and Fe^{2+} states are the least preferred oxidation states (K_3FeO_4 is the only compound with formal Fe^{5+} ions and similarly FeO, $Rb_6Fe_2O_5$, $K_6Fe_2O_5$, $Cs_6Fe_2O_5$, and $Rb_4K_2Fe_2O_5$ with Fe^{2+} ions). Also, only a few compounds with Fe^{4+} ions are so far reported. A first glance at Table I suggests that materials with a higher oxidation state indeed have shorter $d_{Fe\text{-}O}$ (2.162 for Fe^{2+} vs 1.720 Å for Fe^{5+}).

The $d_{Fe\text{-}O}$ depends not only on the oxidation state but also on various other factors, as discussed below. The prominent external factors influencing $d_{Fe\text{-}O}$ for a particular oxidation state are temperature and pressure. For example, in $GdFeO_3$, though Fe remains octahedrally coordinated with a formal 3+ state, the $d_{Fe\text{-}O}$ varies between 2.027 and 2.050 Å between 4 and 230 K (Ref. 8) and shrinks to 1.986 Å when subjected to a pressure of 80 kbar at room temperature.[9]

TABLE I. Formal oxidtation state (valence), number of oxygen ions coordinated to Fe [coordination number (CN)], number of compound entries in the ICSD database (Ref. 6) (entries), and calculated average Fe-O bond length (bond length; in Å) for Fe based oxides.

Valence	CN	Entries	Bond length
5+	4	1	1.720
4+	6	44	1.925
4+	4	4	1.807
3+	2	1	2.125
3+	4	177	1.875
3+	5	19	2.031
3+	6	218	2.032
3+	7	2	2.026
3+	8	5	1.984
3+	9	4	2.006
2+	6	6	2.162

Further, $d_{\text{Fe-O}}$ also depends on the character of the cation coordinated to the FeO_n polyhedra. For example, if the cation contains a lone pair, such as Bi in $Bi_2Fe_4O_9$,[10] the $d_{\text{Fe-O}}$ in the $Fe^{3+}O_6$ unit becomes smaller (1.952 Å) than that in a system without such a lone pair. Moreover, if the other cation possesses a d^0 ion such as Ti^{4+}, Nb^{5+}, or W^{6+}, such constituents participate in a covalent bonding, which shortens $d_{\text{Fe-O}}$, e.g., $d_{\text{Fe-O}}$ in WFe_2O_6 is only 1.919 Å.[11] The average $d_{\text{Fe-O}}$ also depends on the size of the other cation. For example, the cation radii for Ca^{2+}, Sr^{2+}, and Ba^{2+} in an octahedral coordination are 1.14, 1.32, and 1.49 Å, respectively.[12] In $CaFeO_3$, $SrFeO_3$, and $BaFeO_3$, one can explicitly assign the formal oxidation state for Fe to 4+. If $d_{\text{Fe-O}}$ really should reflect a common value for the oxidation state 4+, all these three compounds should have exhibited the same $d_{\text{Fe-O}}$ value. However, the measured $d_{\text{Fe-O}}$ are 1.921, 1.925, and 1.995 Å for $CaFeO_3$, $SrFeO_3$, and $BaFeO_3$, respectively,[13,14] which clearly reflect the important influence of the alkaline-earth ion radius on $d_{\text{Fe-O}}$.

Ionic radius not only depends on the valence of the ions but also on their spin state. Generally, the ionic radius will be larger in the high-spin (HS) state than in the intermediate spin (IS) or low-spin (LS) state due to the magnetovolume effect.[15] Correspondingly the bond length will also depend on the spin state of the ions. For example, Fe^{2+} is octahedrally coordinated with sulfur in both FeS and FeS_2 where Fe is in the HS and LS states, respectively. Correspondingly, the calculated Fe-S bond length in FeS is much longer than that in FeS_2 (2.453 vs 2.255 Å). Partial covalence of the Fe-O bonds can also significantly reduce $d_{\text{Fe-O}}$. For example, due to the covalence effect, some of the Fe-O bond lengths in the $Fe^{3+}O_6$ structural subunit of $FeAlO_3$ and $FeGaO_3$ become as short as 1.847 and 1.868 Å, respectively.[16,17]

From these analyses and additional arguments presented in Refs. 1 and 2, it is clear that $d_{\text{Fe-O}}$ depends not only on the oxidation state of Fe but also on various other factors discussed above. So, one cannot use $d_{\text{Fe-O}}$ alone to deduce the charge state of Fe.

A. Inverse versus normal spinel behavior in Fe_3O_4

Fe_3O_4 is one of the well studied systems that is believed to be in an inverse-spinel structure, i.e., one of the Fe^{3+} ions and an Fe^{2+} ion occupying octahedral sites and the other Fe^{3+} ion occupying the tetrahedral site.[19] However, the following analysis made during the exploration of the valence state aspect of Fe in oxides indicates that Fe_3O_4 can also be considered as a normal spinel where the Fe^{3+} ions are in the octahedral sites and the Fe^{2+} ions are in the tetrahedral site. The calculated[18] electronic structure and magnetic properties for ferrites such as $MnFe_2O_4$, $FeFe_2O_4$, $CoFe_2O_4$, $NiFe_2O_4$, and $ZnFe_2O_4$ based on density-functional theory show that the magnetic moment for ions in the octahedral sites are the same ($3.63\mu_B$/Fe in Fe_3O_4). If one agrees that one Fe^{3+} and one Fe^{2+} are occupying the octahedral site (i.e., if we believe in the inverse spinel picture) then different magnetic moments for Fe in the octahedral sites should be obtained. However, the magnetic moment for Fe at the tetrahedral site is different from that at the octahedral sites ($3.37\mu_B$/Fe in Fe_3O_4), indicating that all Fe ions at the octahedral sites should have the same valence state, i.e., Fe_3O_4 is a normal spinel.

Further, among the five ferrites mentioned above, one can unambiguously assign the valence state of Zn as 2+ in $ZnFe_2O_4$. The structural analysis[20] shows that the divalent Zn occupies the tetrahedral site and the octahedral sites are occupied by Fe^{3+} ions. If one believes that all these systems behave the same way, one should expect Fe^{2+} ions to be in the tetrahedral site and not in the octahedral site in Fe_3O_4, i.e., it could be a normal spinel. Also, it is well established that both Mn_3O_4 and Co_3O_4 are normal spinel, and hence, it would be unusual if Fe_3O_4 behaves as an inverse spinel.

Now, we take a general chemical viewpoint for Fe_3O_4. We have two Fe^{3+} and one Fe^{2+} ions that should be distributed into two octahedral sites and one tetrahedral site within the same structural framework. It will be highly unexpected if ions with the same valence state prefer to occupy sites with different oxygen coordinations even though sites with the same oxygen coordination are available for both the Fe^{3+} ions within the structural framework. So, both Fe^{3+} ions prefer to occupy the two octahedral sites and the Fe^{2+} ion occupies the tetrahedral sites, i.e., Fe_3O_4 should take a normal spinel structure according to the simple chemical picture mentioned above.

Fleet[21] clearly pointed out the reasons behind why Fe_3O_4 is called as inverse spinel as summarized below: The inverse-spinel configuration was originally suggested by Verwey and de Boer[22] to account for the anomalously high electrical conductivity of magnetite. It may be noted that the inverse-spinel idea was a suggestion to interpret the large electrical conductivity and it is not from any direct experimental observation. If it is an inverse spinel, one could perhaps expect different Fe-O bond lengths for the Fe ions at the octahedral site. However, such features were not observed from structural measurements and it was assumed that the relaxation time for electron hopping is appreciably less than that expected for Fe^{2+}-O and Fe^{3+}-O bonds and it may be the reason for the nonobservation of different Fe-O bond lengths at the octahedral sites. As mentioned by Fleet[21] experimental

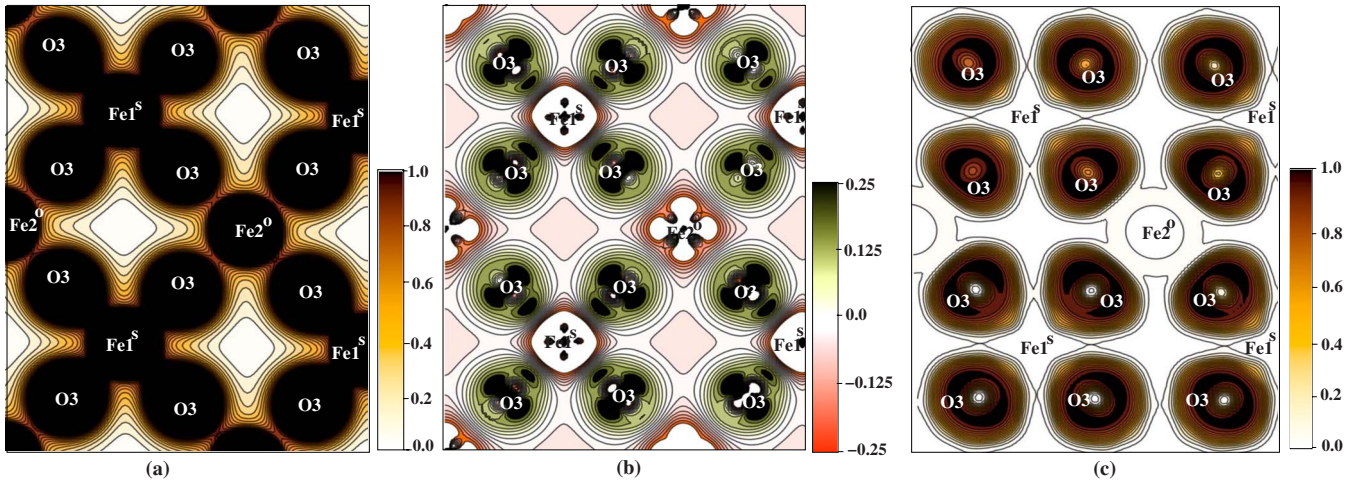

FIG. 1. (Color online) Calculated (a) charge density (in e $Å^{-3}$), (b) charge transfer (in e $Å^{-3}$; red and black colors indicate electron depleted and accepted regions), and (c) electron localization function along the base of the coordination polyhedra of $Sr_4Fe_4O_{11}$. $Fe1^s$ and $Fe2^o$ are Fe in square-pyramidal and octahedral coordinations, respectively.

structural measurements, at room temperature, suggest that natural magnetite has a defect structure. This defect structure could also explain the observed anomalously high electrical conductivity in Fe_3O_4 rather than the inverse-spinel feature suggested by Verwey and de Boer.[22]

To summarize, the inverse-spinel idea was based on suggestions and assumptions rather than any direct experimental observations. Further, this idea was not supported by theoretical calculations, and hence, Fe_3O_4 can be reclassified as a normal spinel.

III. COMPUTATIONAL DETAILS

The relativistic correction to the Schrödinger equation affects the electronic wave function primarily in the vicinity of the nucleus, and hence, it may have impact on hyperfine interactions even for relatively light elements. So, we have taken into account all relativistic effects including spin-orbit coupling in our calculations. Further, the calculations correspond to the experimental situation at 0 K and the absence of external fields and pressure.

We have performed additional calculations which take into account intra-atomic Coulomb repulsion between electrons in $3d$ states with different magnetic quantum number m_l by using the so-called orbital-polarization correction.[23] Thus, the orbital moment was calculated by including spin polarization, orbital polarization, and spin-orbit interaction corresponding to including Hund's first, second, and third rules, respectively. More details about the computational details of the present study can be found in Ref. 1.

The Born effective charge (BEC) calculations were performed using the Vienna *ab initio* simulation package[24] (VASP) within the projector augmented-wave method,[25] as implemented by Kresse and Joubert.[26] The Kohn–Sham equations[27] were self-consistently solved using an iterative matrix diagonalization method. This is based on a band-by-band preconditioned conjugate-gradient[28] method with an improved Pulay mixing[29] to efficiently obtain the ground-state electronic structure. The forces on the atoms were calculated using the Hellmann–Feynman theorem and these were used to perform a conjugate-gradient relaxation. Structural optimizations were continued until the forces on the atoms had converged to less than 1 meV $Å^{-1}$ and the pressure on the cell had minimized within the constraint of constant volume.

IV. OXIDATION STATE OF Fe FROM CHEMICAL BONDING

In order to gain more insight into the bonding interaction between the constituents and their oxidation state, additional analyses of charge density, charge transfer, electron localization function, Born-effective charges, partial density of states, and crystal orbital Hamilton population were made.

The electron density calculated by VASP is displayed in Fig. 1(a) for a plane containing the $Fe1^s$, $Fe2^o$, and O atoms. This clearly shows that the bonding interaction between Fe and O is not purely ionic. The directional nature of the charge-density distribution between Fe and O indicates the presence of covalent character in the bonding. The charge transfer distribution in Fig. 1(b) shows that electrons are transferred from both Sr (not shown) and Fe to the O sites, which is consistent with the ionic picture. If the bonding interaction between Fe and O had been purely ionic, one would expect an isotropic charge transfer distribution. The anisotropic distribution of the charge transfer thus confirms the presence of a finite covalent component in the bonding.

ELF can distinguish between different bonding interactions in solids.[30] The small value of ELF between the atoms in Fig. 1(c) confirms the presence of dominant ionic bonding in $Sr_4Fe_4O_{11}$. The ELF distribution also shows maxima at the O sites and minima at the Fe and Sr sites (not shown), once more confirming the charge transfer from Sr and Fe to the O sites. Moreover, polarization of ELF at one O site toward other O sites indicates hybridization interaction. The conclusion from the charge density, charge transfer, and ELF analy-

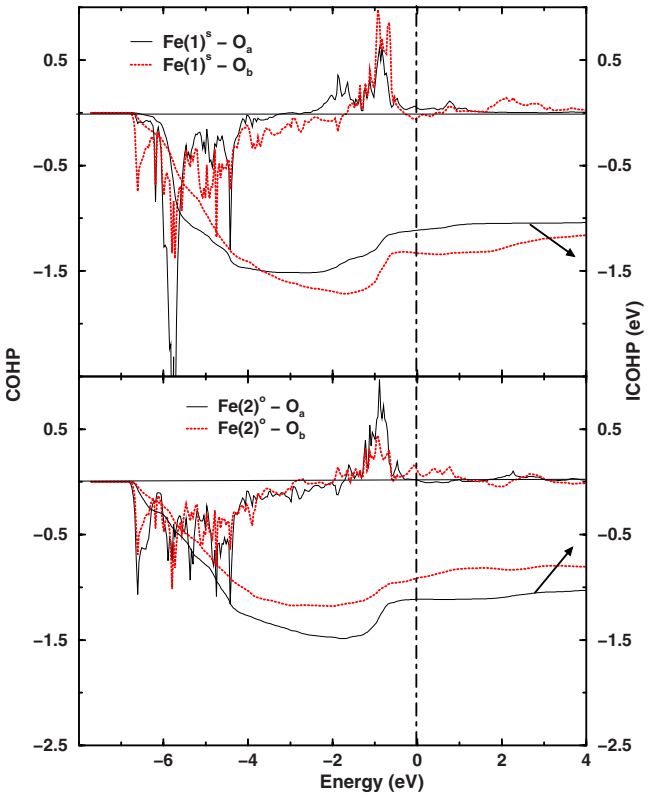

FIG. 2. (Color online) COHP and ICOHP for Fe-O in $Sr_4Fe_4O_{11}$. Fe1^s and Fe2^o are Fe in square-pyramidal and octahedral coordinations, respectively. Oa and Ob refer to oxygen atoms in the apical and base of the polyhedra.

ses is accordingly that the bonding interaction between Sr and O as well as between Fe and O has dominant ionic character with finite covalent components. This is consistent with the conclusions arrived at from the Born-effective charge analysis discussed below. All these results clearly establish the mixed ionocovalent character of the bonding in $Sr_4Fe_4O_{11}$.

The crystal orbital Hamiltonian population (COHP) is the density of states weighted by the corresponding Hamiltonian matrix element, which was calculated here using the tight binding linear muffin-tin orbital program (TBLMTO).[31] COHP is an indicator of the strength and nature of bonding (negative COHP) or antibonding (positive COHP) interactions.[32,33] The COHP analyses were made using the TBLMTO formalism where the spin-orbit coupling and orbital-polarization corrections are not considered in the calculation. This may influence the quantitative conclusion arrived about the Fe-O bond strength. The calculated COHP for the Fe1^s-Oa, Fe1^s-Ob, Fe2^o-Oa, and Fe2^o-Ob interactions in $Sr_4Fe_4O_{11}$ (a denotes apical and b denotes basal plane interactions) is shown in Fig. 2. The COHP curves reveal that all bonding states for the Fe-O interactions are within the valence band from around −2 eV below the Fermi level. The FeO_6 octahedra are highly distorted and hence the Fe2-Oa bond energy (−1.103 eV; defined as the integrated COHP up to the Fermi level) is stronger than the Fe2-Ob bond energy (−0.923 eV). The Fe1-O bonding interaction along the base of the square pyramid (−1.339 eV) is stronger than that along the apex (−1.123 eV). The considerable difference in the ICOHP values for the Fe-O bonding interactions indicate that the Fe ions indeed are in two different valence states.

In high-symmetry oxides with a simple structure, the oxygen Born-effective charge (Z^*) is isotropic and close to −2.[34] Owing to the site symmetries involved, the diagonal components of Z^* are anisotropic for all ions in $Sr_4Fe_4O_{11}$ (Table II). If ions have a closed-shell-like character, each ion should carry an effective charge close to its nominal ionic value (according to a rigid-ion picture). Owing to covalence effects, large amounts of nonrigid delocalized charge flow across the lattices during displacements of the ions.[35,36] Consequently, one will obtain effective charges much larger than the nominal ionic values. The charges on Sr and O are larger than they would have been according to a pure ionic picture. This reveals the presence of a large dynamic contribution superimposed on the static charge. Similar giant values of Z^* have been reported for other perovskite-related oxides[36,37] by using quite different technical ingredients.

The BEC is indeed a macroscopic concept,[38,39] involving the polarization of the valence electrons as a whole, while the charge "belonging" to a given ion is a poorly defined concept. The high BEC values in Table II indicate that relative displacements of neighboring ions against each other trigger a high polarization. Roughly speaking, a large amount of nonrigid, delocalized charge is responsible for higher values of BEC than the nominal charges. From the Table II, it is again clear that both Sr and Fe donate electrons and O accepts electrons, which is consistent with the traditional ionic picture. It can be recalled that for a pure ionic system, one could expect a more isotropic character of Born-effective charges. Considerable anisotropy in the diagonal components of BEC (Table II) and noticeable off-diagonal components at the oxygen sites (not given) confirm the presence of covalent

TABLE II. Calculated diagonal elements of the Born-effective-charge tensor (Z^*_{ij}) for $Sr_4Fe_4O_{11}$ in the ground-state *G*-AF configuration.

Atom	Z^*_{xx}	Z^*_{yy}	Z^*_{zz}	Average
Sr	2.554	2.919	2.127	2.533
Fe1^s	4.540	4.669	1.422	3.544
Fe2^o	6.909	6.006	4.667	5.861
O1	−2.174	−2.368	−4.718	−3.087
O2	−2.841	−2.361	−4.275	−3.153
O3	−3.827	−3.252	−1.504	−2.861

TABLE III. The calculated spin (μ_{spin}) and orbital (μ_{orb}) moments (in μ_B atom^{-1}) and calculated and experimental hyperfine field parameters (in T) for $Sr_4Fe_4O_{11}$ and related oxides.

				B_{FC}							
Compound	Atom	μ_{spin}	μ_{orb}	B_{val}	B_{core}	$B_{FC,tot}$	B_{dip}	B_{orb}	$B_{HF,tot}^{theor}$	$B_{HF,tot}^{ad\ hoc}$	$B_{HF,tot}^{expt.}$
$Sr_4Fe_4O_{11}$	$Fe1^s$	2.86	0.01	18.782	−35.825	−17.043	5.55	1.44	−10.04	−20.79	
	$Fe2^o$	3.53	0.04	16.262	−45.778	−29.508	−1.52	−1.86	−32.88	−46.62	45
$SrFeO_3$	Fe^o	2.89	0.15	10.225	−36.119	−25.894	0.13	0.82	−24.94	−35.77	33
$Sr_2Fe_2O_5$	$Fe1^o$	3.21	0.04	26.110	−42.723	−16.613	−1.24	2.62	−15.23	−28.05	54
	$Fe2^o$	3.38	0.02	28.584	−43.229	−14.645	−2.77	−1.57	−18.98	−31.95	45
$Sr_3Fe_2O_6$	Fe^s	3.33	0.05	25.559	−43.970	−18.410	4.45	3.54	−10.42	−23.61	52
$LaFeO_3$	Fe^o			8.903	−47.269	−38.367			−38.36	−52.54	56

bonding formed by the O-2p and Fe-3d orbitals. The covalent bonding between Fe and O could explain the presence of anomalous contributions (defined as the additional charge compared to the ionic value) to the effective charge at the Fe and O sites. The calculated average diagonal component of the BEC in Table II is less than 4 at $Fe1^s$ and larger than 4 at $Fe2^o$, justifying the assignment of the formal valence of $Fe1^s$ and $Fe2^o$ as 3+ and 4+, respectively. As additional evidences for the assignment of 3+ and 4+ states for $Fe1^s$ and $Fe2^o$, respectively, we presented in our reply to comment[2] integrated DOS data (Fig. 1 of Ref. 2) which document that the $Fe1^s$ site carries more positive charge than the $Fe2^o$ site.

V. OXIDATION STATE FROM MÖSSBAUER DATA

Mössbauer spectroscopy provides an extremely local probe for mapping changes in the charge and spin density around an atom and thus offers the possibility of getting information about individual spatial spin configurations. Both the electron contact density and the electric field gradient are rather singular quantities, which measure the properties of the electron gas at an extreme point (the position of the nucleus), which is far from the region where the chemical bonding rules. However, these quantities are significantly influenced by the chemical bond. However, the extraction of the Mössbauer parameters from experimental measurements for complex materials with different crystallographic sites is often difficult as the information from these experiments are rather difficult to interpret and far from transparent. Therefore, reliable theoretical calculations are highly needed in order to provide a firmer basis for the understanding of the experimentally measured Mössbauer parameters. With the availability of high speed computers and the development of new techniques for electronic structure calculations, it has become possible during recent years to supply a first-principles description of the Mössbauer parameters. Now, let us provide a brief description of Mössbauer parameters from first-principles calculations.

A. Hyperfine field

The utilization of the magnetic hyperfine field (HF) (B_{HF}) as a local probe of magnetism is based on the empirical fact that B_{HF} is, to a good approximation, proportional to the local magnetic moment. The magnetic moment of the two nonequivalent Fe sites in $Sr_4Fe_4O_{11}$ differs by $0.673\mu_B$, which is in accordance with the differences in the local environment. This has important consequences for the variation in B_{HF} between different sites within the unit cell of $Sr_4Fe_4O_{11}$. The HF can be expressed as a sum of four contributions: (1) the Fermi contact term (B_{FC}) arising from the nonzero spin density at the nucleus, (2) the dipolar (B_{dip}) magnetic field produced by the on-site spin density, (3) the orbital term (B_{orb}) stemming from the magnetic field produced by the current flowing around the nucleus, the magnitude of which is proportional to the orbital moment, and (4) the lattice contribution (B_{lat}), which represents the dipolar field originating from the moments residing on the other lattice sites. Sometimes, other terms besides B_{FC} decide the total HF ($B_{HF,tot}$) at a particular site. This makes it difficult to assign the measured HF to a particular site for systems with more than one site occupied by magnetic constituents. In such cases, a theoretical approach may be useful for the unambiguous assignment.

As theoretical knowledge about the different contributions is important for the understanding of the development of $B_{HF,tot}$ at different sites in mixed valent systems, we have calculated various contributions to the HF for $Sr_4Fe_4O_{11}$ and related oxides. The calculated data are listed in Table III, together with the local spin and orbital moments at each Fe site. Compared to the corresponding findings for the related compounds, the calculated $B_{HF,tot}$ values for $Sr_2Fe_2O_5$ and $Sr_3Fe_2O_6$ appreciably deviate from the experimentally reported values. As the calculated isomer shift (see Table IV) at the Fe sites in these two compounds are in good agreement with experimental findings, the deviations for the theoretical $B_{HF,tot}^{theor}$ appears to be introduced by the assumption of a simple AF structure for the computations which in turn gives rise to an incorrect contribution from the valence electrons (B_{val}; see below).

As the most prominent contribution to $B_{HF,tot}$ is B_{FC}, we will now analyze this term in more detail. According to relativistic description, B_{FC} (in T) is proportional to the spin density averaged over the Thomson spheres centered at the Fe nuclei:[40]

TABLE IV. Calculated and experimental (given in parentheses) Mössbauer parameters for $Sr_4Fe_4O_{11}$ and related oxides.

Compound	Atom	Δ_{IS} (mm s^{-1})	EFG (10^{21} V m^{-2})	η	Δ_Q (mm s^{-1})
$Sr_4Fe_4O_{11}$	$Fe1^s$	0.136 (−0.03)	1.623	0.706	0.146 (0.35)
	$Fe2^o$	0.572 (0.47)	−5.201	0.089	−0.434 (−0.67)
$SrFeO_3$	Fe	0.291 (0.15)	1.617	0.001	0.135
$Sr_2Fe_2O_5$	Fe1	0.649 (0.49)	4.779	0.452	0.411
	Fe2	0.361 (0.29)	9.363	0.773	0.854
$Sr_3Fe_2O_6$	Fe	0.522 (0.48)	3.787	0.000	0.315
$LaFeO_3$	Fe	0.620 (0.47)	−0.583	0.622	−0.052

$$B_{FC} = \frac{2}{3}\mu_0 g_e \mu_B s \int_0^{r_T} [\rho_s^{\uparrow}(r) - \rho_s^{\downarrow}(r)]dr$$

where g_e is the electron gyromagnetic constant and $s=1/2$. The radius of the Thomson sphere $r_T=Ze^2/4\pi\epsilon_0 m_e c^2$ is much larger than the radius of the nucleus (r_N; for Fe, $r_T=72\times10^{-15}$ m whereas $r_N=4\times10^{-15}$ m).

For simplicity, B_{FC} can be split into a core-polarization contribution (B_{core}) and a valence contribution (B_{val}). The dominant interaction for B_{core} at the Fe site is the exchange coupling of the inner core s shells with the $3d$ orbitals of the probe atom. Because of shielding effects, the influence of the magnetic moments of neighboring atoms on B_{core} is negligible. Accordingly, B_{core} is proportional to the local magnetization. On Fe, the $1s$ and $2s$ electrons lie spatially inside the $3d$ electrons, while the $4s$ electrons are outside the $3d$ shell. Therefore, the spin polarization of $1s$ and $2s$ will be opposite to the polarization of $4s$, leading to orientation of B_{core} opposite to the $3d$ moment for the $1s$ and $2s$ electrons and a $4s$ contribution that tends to cancel the $1s$ and $2s$ contributions. The $2s$ and $4s$ contributions are larger than the $1s$ contribution because these orbitals are spatially closer to the $3d$ orbitals and hence exhibit stronger exchange interaction. The $3s$ and $3d$ orbitals overlap leads to competing and mutually cancelling tendencies,[41] but the $3s$ contribution will be small and can be neglected in a qualitative discussion.

The B_{core} arising from the intra-atomic s-d exchange is expected to linearly vary with the local spin moment but with the opposite sign. This is indeed confirmed by our calculations. Importantly, the total HF is decided by the B_{core}. However, the local-density approximation does not allow an accurate calculation of the HF, e.g., in the case of Fe, core contributions seem to be underestimated by about 30%.[40,42] It seems especially important to improve the description of the core states, in contrast to many other problems in condensed matter physics for which the valence states and the nature of the chemical bonding are of prime interest. As the generalized gradient approximation (GGA) is based on the expression for the exchange-correlation energy of the homogeneous electrons gas (depending on the density as proportional to $\rho^{1/3}$ at high electron density), it fails to treat the exchange splitting caused by the deformation of the wave function imposed by the s-d exchange interaction (core polarization). Thus, the calculated B_{core} will always be smaller than the experimental value. The self-interaction correction[43] is especially important for the bound core states in order to obtain a reliable value for the core hyperfine field. Several approaches have been introduced in attempts to meet this challenge and some improvement has indeed been made.[44] However, we adopted an *ad hoc* procedure by scaling the calculated B_{core} by a factor of 1.3 in order to reproduce the experimentally measured HF values. Linear fits of B_{core} vs local moment gave the conversion constants of −12.5 T μ_B^{-1} and −12.95 T μ_B^{-1} for the $Fe1^s$ and $Fe2^o$ sites, respectively. These values are close to theoretical values in the range from −10.0 T μ_B^{-1} to −12.5 T μ_B^{-1} reported by Ebert *et al.*[45,46] for Fe_xT_{1-x} with T=Co, Cr, and Ni.

Although the contribution from B_{val} to the hyperfine field of the magnetic atom is normally small, it is very important for the understanding of the local electronic and magnetic properties of a system due to its sensitivity to the interactions with neighbors. It is suggested[47] that the B_{val} can be denoted as

$$B_{FC,val} = A\mu_{4s}(i) + \sum_j D_{ij} n_{ij} \mu(j),$$

where $\mu_{4s}(i)$ is the on-site $4s$ magnetic moment of the ith atom, n_{ij} and $\mu(j)$ are the number and moment of the neighboring j-site magnetic atoms, and A and D_{ij} are hyperfine coupling constants related to hybridization interactions and moments at both the Fe and O sites. The first term ($B_{val,loc}$) is positive and arises from the local valence electrons, the value of which depends on the $3d$ moment at the probe site. The second term ($B_{val,tr}$) is due to the transferred contribution, which is either positive or negative. Since $B_{val,tr}$ originates from the conduction electrons which are polarized via the RKKY interaction, it depends on the moment, the magnetic coupling, and the configuration of the neighboring atoms. It increases with increasing number of ferromagnetically coupled surrounding Fe atoms and decreases with the number of AF coupled surrounding Fe atoms.[48] The large positive value of B_{val} (Table III) indicates that $B_{val,loc}$, and hence the local $3d$ moment, plays an important role in deciding B_{val}. In general, if Fe-O distances are large, the hyperfine coupling between the atoms concerned will be weaker, resulting in a smaller $B_{val,tr}$ for constant magnetic moments on the neighboring sites. So, the transferred HF at the $Fe1^s$ site will be larger than that at the $Fe2^o$ site for $Sr_4Fe_4O_{11}$. The

coupling is of AF character and leads to a negative partial 4*s* magnetic moment for the probe atom.

The net total magnetic moments from the oxygen ions surrounding $Fe1^s$ and $Fe2^o$ site are $0.363\mu_B$ and $0.218\mu_B$, respectively. The average Fe1-O distance is shorter (1.874 Å) than the average Fe2-O distance (2.032 Å), which is in consistent with our chemical bonding analysis that the hybridization interaction between $Fe1^s$ and O is relatively stronger than that between $Fe2^o$ and O. The larger positive value of $B_{\mathrm{val,tr}}$ for $Fe1^s$ is an effect of the increase in the magnetic polarization of the oxygen atoms which (via repopulation) enhances the spin polarization of the 4*s* states of the $Fe1^s$ atoms despite the small local moment at this site compared to the $Fe2^o$ site. Effectively, the positive $B_{\mathrm{val,tr}}$ added to the positive $B_{\mathrm{val,loc}}$ contribution produces a relatively large positive value for B_{val} at the $Fe1^s$ site. As a result, the numerical value of $B_{\mathrm{FC,tot}}$ at the $Fe1^s$ site becomes much smaller than that at the $Fe2^o$ site (see Table III). The local *s* magnetic moments at the $Fe1^s$ and $Fe2^o$ sites are only $0.018\mu_B$ and $0.017\mu_B$, respectively. Generally speaking, the bonding states induced by *s*-*d* hybridization produce a negative contribution to $B_{\mathrm{FC,val}}$, while the antibonding states lead to a positive contribution to the same. It may thus be inferred that the larger number of *d* electrons at $Fe1^s$ have enhanced the *s*-*d* hybridization, resulting in a larger specific spin polarization of the valence *s* electrons at the nucleus in spite of the fact that the magnetic moment of $Fe1^s$ is smaller than that of $Fe2^o$.

The calculated $B_{\mathrm{FC,val}}$ for both Fe sites in $Sr_4Fe_4O_{11}$ is positive despite the moments at the considered sites being positive, indicating that the hyperfine coupling constants are positive as a result of the antibonding Fe-O states.[49] As B_{val} and B_{core} are of opposite sign, the sum represents a decreases in the magnitude of the total HF.

For the calculation of B_{dip} and B_{orb}, the method of Blügel *et al.*[40] was employed. The dipolar term is defined as

$$B_{\mathrm{dip}} = \mu_B \langle \psi | \frac{1}{r^3} \left[\sigma \cdot \mu_N - 3 \left(\sigma \cdot \frac{\mathbf{R}}{r} \right) \left(\mu_N \cdot \frac{\mathbf{R}}{r} \right) \right] | \psi \rangle,$$

where μ_N is the magnetic dipole moment, σ is the spin index, and ψ is the solution of the Dirac equation determined for a potential $V(\mathbf{R})$, $0 \leqslant \mathbf{R} \leqslant \infty$. First, the dipolar HF does not depend on the direction of motion of an electron, so that $\pm m$ orbitals yield the same dipolar HF. Second, B_{dip} explicitly depends on the electron spin, such that an electron with opposite spin in the same orbital *m* yields an opposite field. The spin dipole contribution at the Fe1 and Fe2 sites are 5.553 and −1.521 T, respectively.

The orbital contributions to the magnetic moment as well as to the HF are caused by an unquenching of the orbital moment due to spin-orbit coupling. The orbital contribution to the HF is very sensitive to the local symmetry. Because the hyperfine interaction takes place in the vicinity of the nucleus, where relativistic effects such as the mass-velocity enhancement, the Darwin term, and the spin-orbit coupling have their strongest influence on the electronic wave functions, it is expected that these effects are also quite important for the hyperfine interaction. The orbital contribution to the HF is defined as

$$B_{\mathrm{orb}} = -\mu_N \frac{e}{mc} \langle \psi | \frac{\mathbf{L}}{r^3} | \psi \rangle,$$

where $\mathbf{L}$ is the orbital momentum. Orbitals with opposite quantum number *m* yield opposite B_{orb} because in orbitals with opposite *m*, the electrons move in opposite directions due to the different orientations of the angular momenta. In some cases B_{orb} is positive and comparable to B_{FC}, and hence, the resulting HF is smaller than that originating from the FC term alone.[50] In some cases, B_{orb} is much larger than B_{FC} and the net HF will then be decided by the orbital moment.[51] The B_{orb} can be obtained by including spin-orbit coupling into the calculation in addition to the spin polarization. Because the spin-orbit-induced orbital moment of iron is generally affected by electron-electron interactions, such calculated orbital moments usually come out much smaller than the experimentally measured values.[52] By including Hund's second rule (through the orbital-polarization correction[23]), one can remedy this deficiency. The calculated orbital moment at the $Fe1^s$ and $Fe2^o$ sites is $0.007\mu_B$ and $0.041\mu_B$, respectively, and these values are much smaller than that experimentally found for elemental Fe [$0.08\mu_B$ (Ref. 53)]. The influence of the orbital moment on HF is much larger than that between the spin moment and the core-polarization part of the FC term ($B_{\mathrm{FC,core}}$). Hence, even though the calculated orbital moment at the $Fe1^s$ and $Fe2^o$ sites are small, the B_{orb} takes the non-negligible values of 1.435 and −1.859 T for $Fe1^s$ and $Fe2^o$, respectively.

The lattice contributions, which are typically small in ferromagnets and even smaller in antiferromagnets, are calculated to be 8×10^{-3} and 9×10^{-3} T for $Fe1^s$ and $Fe2^o$, respectively.

The above detailed analysis of various contributions to the HF clearly shows that B_{core} is the deciding factor for the HF at both Fe sites in $Sr_4Fe_4O_{11}$ and this parameter is directly related to the corresponding magnetic moments. The charge state of an ion is decided by the total charge density at each site. On the other hand, the measured HF of an ion reflects the spin density which is the difference between the majority- and minority-spin electrons at the site concerned. As the spin density is independent of the total charge density and dependent on the exchange interaction, the measured HF at the Fe sites in $Sr_4Fe_4O_{11}$ cannot provide information about the charge state of the iron atoms.

B. Isomer shift

The nucleus and its electrons interact in several ways, the most obvious being the electrostatic attraction. If the nuclear charge distribution in iron (^{57}Fe) is the same for the $I=1/2$ ground state and the $I=3/2$ excited state, then the electrostatic energy of the system comprising electrons plus nucleus would be the same for both states. In fact, the excited ^{57}Fe nucleus is 0.1% smaller in radius than the ground-state nucleus, which causes the Mössbauer transition energy to depend on the electron density at the nucleus. This effect produces a so-called isomer shift (Δ_{IS}) of the Mössbauer spectrum. The Δ_{IS} reflects the *s*-electron probability density at the nucleus since only the *s* partial waves extend into the

nuclear regime. Mainly two terms contribute to the IS; one is the contact density coming from 4*s*-like electrons in the conduction band $[\rho_{4s}(0)]$ and the other contribution originates from the shielding effect on the 3*s* electron density $[\rho_{3s}(0)]$ by the modified 3*d*-like band electrons.

It is often problematic to assign the experimentally observed Δ_{IS} to the respective atomic sites in mixed valent systems.[54] Hence, we have used density-functional calculations to estimate Δ_{IS} for the Fe sites in $Sr_4Fe_4O_{11}$ and a few related compounds.

The isomer shift of a nuclear transition energy is given by

$$\Delta_{IS} = \alpha[\rho_a(0) - \rho_s(0)], \quad (1)$$

where ρ_a and ρ_s are the electron charge density at the nuclear positions (the contact densities) in the absorber (a) and the source (s) material, respectively. If Δ_{IS} is measured as the velocity of the absorber relative to the source materials, the calibration constant α of Eq. (1) is given by

$$\alpha = \beta\Delta\langle r^2\rangle,$$

where β is another numerical constant and $\Delta\langle r^2\rangle$ is the difference between the mean square radius of the Mössbauer nucleus in its excited and ground states. The value of α depends only on the probe nucleus and can be determined from comparison between results from band structure calculations and actual experimental determinations of the isomer shift. In order to calculate Δ_{IS} from the difference in electron contact density between the source and absorber, we have derived the calibration constant by using the calculated charge density at the Fe nucleus $[\rho(0)]$ for several compounds with different chemical bonding characters and established the linear relation between $\rho(0)$ and the experimentally measured Δ_{IS} values. The electron contact density was calculated as the average electron density in the nuclear volume defined by a sphere of radius $R=1.2A^{1/3}$ fm (where A refers to the mass number).

The Δ_{IS} values listed in Table IV are given relative to α-Fe and refer to the low temperature. The experimental accuracy is not quoted but is typically of the order 0.01–0.05 mm s^{-1}. However, the calculated values are subject to systematic errors, which are difficult to assess, for example, the validity of GGA. The degree of agreement between experimental and theoretical values may be judged from plots of the experimental Δ_{IS} vs theoretical electron contact density, as shown in Fig. 3. The straight line through the points in Fig. 3 confirm the linear relationship, whereas the scatter around the line reflects the combined experimental and theoretical uncertainties. The calibration constant derived from the best linear fit of Eq. (1) is $\alpha = -0.360$ mm s^{-1}. As seen from Table IV, Δ_{IS} for $Fe1^s$ is smaller than that for $Fe2^o$.

The shorter $Fe1^s$-O bonds allow more spreading of the 3*d* electrons into the oxygen site region which reduces the 3*d*-3*s* shielding effect. The calculated *s*, *p*, and *d* electron charges within the atomic sphere are 0.471, 0.743, and 6.019 for $Fe1^s$ and 0.383, 0.578, and 5.867 for $Fe2^o$. The increased number of *d* electrons on $Fe1^s$ causes a shielding of the *s* component of the wave function away from the nuclear region with a resulting lower contact density.[55]

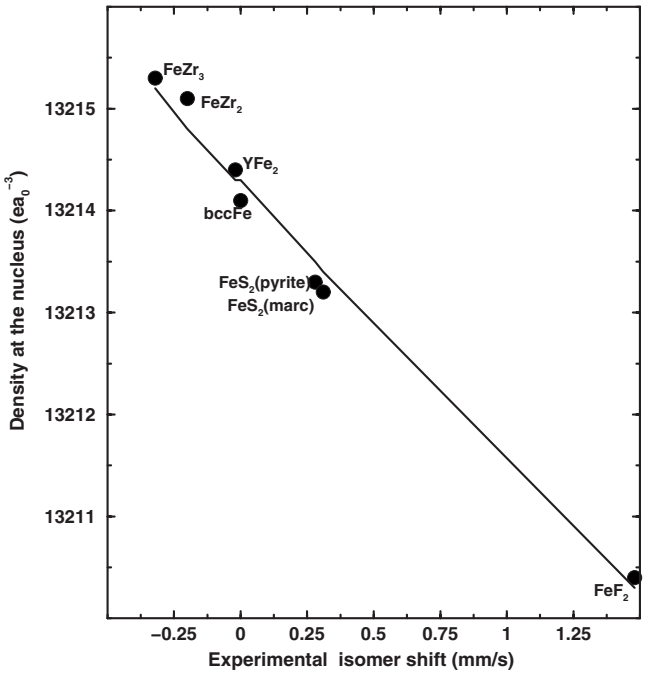

FIG. 3. The calculated contact density at the Fe site versus experimentally measured isomer shift. The line represents a least squares fit to the points.

Another factor contributing to the difference between Δ_{IS} for $Fe1^s$ and $Fe2^o$ is the overlap interaction between 3*d* and 4*s* orbitals. Marshall[56] pointed out that the overlap of the Fe inner shells with ligand wave functions produces a significant change in $\rho(0)$. The mechanism for this change is called the overlap distortion. Due to the spherical symmetry of the 4*s* orbitals, their overlap interaction with the ligands will be larger than that of 3*d* electrons. So, the back donation provides a possible mechanism for a smaller Δ_{IS} at the $Fe1^s$ site than usually found for Fe^{3+} ions. The present study suggests that the covalence of the Fe1-O bond is stronger than that of the Fe2-O bonds, as evidenced by the smaller Δ_{IS} for the $Fe1^s$ site than for the $Fe2^o$ site. This is consistent with our findings for the chemical bonding which shows the stronger covalence character of the Fe1-O bond. The 1*s* and 2*s* electron density at the nucleus is independent of the chemical environment around Fe. However, the 3*d* electrons shield the 3*s* electrons and hence reduces their presence at the nucleus. However, this picture is made more complicated by the involvement of Fe-4*s* character in the bonding orbitals. The 4*s* character also reduces the Δ_{IS}, and usually, it is not clear which of the two effects is dominant.

Let us now analyze the factors that influence Δ_{IS} in more detail. The Δ_{IS} may in principle be used to determine the charge state of iron, but in practice, this parameter is generally not very sensitive for iron compounds with strong covalent bonds.[57] It is well known that on going from Ge to C (diamond), the degree of covalence increases, and, correspondingly, the value of the Δ_{IS} decreases from −0.11 to −0.39 mm s^{-1}.[58] An empirical correlation has been advanced between the covalence of Fe and Δ_{IS} (see, for example, the Δ_{IS} vs ionicity diagram in Ref. 59). From a detailed analysis of various factors which influence Δ_{IS}, Ingalls *et al.*[60] con-

cluded that one should not compare Δ_{IS} for compounds with appreciable covalent character with those having distinct ionic character. Ohashi[61] suggested that increase in the covalent bonding between iron cations and oxygen anions shortens the bond length and takes away electrons from the Fe site and thus results in lowered Δ_{IS}. Moreover, for partially empty $3d$ orbitals, covalence indirectly influences the Δ_{IS} via the screening of the $3s$ and eventually $4s$ electrons.

The value of Δ_{IS} gives a hint about the degree of delocalization of electrons which lowers the $3d$ density compared to high-spin cases. If the delocalization increases the Δ_{IS} becomes smaller. This is clearly demonstrated in the decrease in Δ_{IS} for Fe^{2+} in the following sequences (values in mm s^{-1}; data from Refs. 62 and 63): $FeTe_2$ (0.47), $FeSe_2$(0.39), and FeS_2(0.27), and for Fe^{4+} in $FeSb_2$ (0.45), $FeAs_2$ (0.31), and FeP_2 (0.09).

According to a pure ionic picture, Fe^{4+} should be characterized by a low electron contact density, since a large fraction of the $4s$ electrons are dragged away from the Fe atoms. This causes smaller Δ_{IS} for Fe^{4+} ions than for Fe^{3+} ion in oxides. Such features may have led Adler[3] to believe that Fe^{4+} resides at the square-pyramidal site in $Sr_4Fe_4O_{11}$, as the estimated Δ_{IS} is smaller for this site. However, for compounds with partial covalence, the $4s$ electrons will participate more efficiently in the covalent bonding because of their spherical symmetry. This indicates that if Fe ions at two different sites carry the same formal valence states, Δ_{IS} will be smallest for the species which is involved in the strongest covalent bonding with its neighbors.

The value of Δ_{IS} also depends on external factors such as pressure and temperature; for example, for the Fe^{3+} high-spin case, the Δ_{IS} changes from 0.36 mm s^{-1} at room temperature to 0.48 mm s^{-1} at 4.2 K.[64] (The temperature dependence of Δ_{IS} is usually attributed to the second-order Doppler shift.) Generally, Δ_{IS} also decreases with increasing pressure.[65–68] In $Sr_4Fe_4O_{11}$, the shorter $Fe1^s$-O bond length exerts "pressure" on the $Fe1^s$ sublattice, resulting in a more compressed p electron cloud on the surrounding O atoms, which causes the partial s wave function to diminish at the nucleus (through shielding). On lattice compression, the energy levels of the $4s$ electrons of the transition metals increase faster than the $3d$ electrons due to the larger overlap with the $4s$ orbital. As a consequence, the $4s \rightarrow 3d$ electron transfer will energetically become more favorable which in turn reduces the s electron density at the nucleus. We have also found a significantly smaller moment at the $Fe1^s$ site than at the $Fe2^o$ even though the former carries more valence electrons than the latter. This indicates that the s electrons are more spread out due to the more delocalized character of these electrons and this results in relatively weaker exchange interaction and also smaller Δ_{IS} than that of $Fe2^o$.

For the estimation of $\rho(0)$, knowledge about the occupation of the valence s, p, and d orbitals is not sufficient. One must also take into account the radial and angular perturbations of each occupied valence wave function including direct effects on the core due to the neighbors. Moreover, the contact density depends on the spin state of the ion, a high-spin state having a larger contact density than a low-spin state.[60] In addition, Δ_{IS} depends on the coordination number of Fe. For example, Fe^{3+} in trigonal-planar (Cu_5FeS_4) and tetrahedral coordinations $CuFeS_2$ are 0.37 and 0.23 mm s^{-1}, respectively.[54] The spread in Δ_{IS} for Fe in a particular valence states is so large that, in some cases, it more or less overlaps with the Δ_{IS} of Fe in other valence states. For example, the Δ_{IS} for Fe^{3+} in the oxides spread over a range of about 0.4 mm s^{-1}, which covers a large portion of the Δ_{IS} values often regarded as typical for Fe^{2+} ions.[60] For Fe in one and the same valence state, e.g., Δ_{IS} in tetrahedral coordination in garnets is always smaller than that in octahedral coordination.[69] Here, not only the change in CN but also the difference in the Fe-O distance comes into the picture.

In conclusion, the value of Δ_{IS} is determined by the s electron density at the nucleus, which depends on the degree of localization of the electrons at a particular site (i.e., localized electrons have a large contact density and hence larger Δ_{IS}). Therefore, in addition to the charge state, the coordination number, bond length, spin state, nature of bonding interaction with neighbors, etc., are responsible for the actual size of Δ_{IS} at the site. The changes in the shape of the s electron distribution by shielding and hybridization effects are the main reasons for the variation in Δ_{IS} between the different Fe atoms in $Sr_4Fe_4O_{11}$. Based on our band structure findings, $Fe1^s$ can be formally assigned as Fe^{3+}. However, the presence of strong covalence at $Fe1^s$ reduces $\rho(0)$ and hence Δ_{IS} becomes lower than usually expected for Fe^{3+} ion. Hence, it is not appropriate to take Δ_{IS} of pure ionic compounds as references for assigning charge states of constituents of compounds with partial covalence. It can be said that the magnitude of the Δ_{IS} in the two different Fe sites in $Sr_4Fe_4O_{11}$ rather reflects the strength of their covalent bonding with oxygen. In summary, the charge state of an Fe ion is decided by the valence electrons that consist of the s electrons as well as the p and d electrons. From a detailed analysis of the origin of the isomer shift, it is clear that the isomer shift cannot provide the required information about the total charge density at the probe site which decides the charge state.

C. Quadrupole splitting

The experimentally observed quadrupole splitting (Δ_Q) reflects the quadrupole-quadrupole interaction between the nucleus and the surrounding electron cloud. It can be expressed in terms of the nuclear quadrupole moment and the electric field gradient (EFG), produced by the electrons at the position of the nucleus.[70,71] The quadrupole splitting may provide a rather indirect indication of the valence state, however, it is usually impossible to draw unambiguous conclusions about the charge state from Δ_Q.[57] Since the EFG tensor is directly related to the asphericity of the electron density in the vicinity of the probe nucleus, the quadrupole splitting allows the estimation of covalence and/or ionicity of the chemical bonds in the solid provided the quadrupole moment is known. Unfortunately, if a system contains more than one crystallographic site, experiment does not explicitly reveal which environment corresponds to which EFG.[68] Hence, a theoretical estimation of the EFG for the different sites will help resolve the experimental data.

For an $I=3/2$ to $1/2$ transition, as for ^{57}Fe, the quadrupole splitting is given by

$$\Delta_Q = \frac{1}{2} e|QV_{zz}| \sqrt{1 + \frac{\eta^2}{3}}, \tag{2}$$

where e is the elementary charge, Q is the quadrupole moment of the excited Mössbauer nucleus, and V_{zz} and η are the EFG and asymmetry parameter, respectively. The asymmetry parameter η is a measure of the deviation from uniaxial symmetry, and hence, Δ_Q is a measure of the deviation from cubic symmetry.

The EFG is a traceless symmetric tensor of rank 2, which is defined as the second derivative of the Coulomb potential at the position of the nucleus, viz., $V_{ij} = \partial^2 V^* / \partial x_i \partial x_j$, where V^* is the potential due to electrons in non-s states. The Coulomb potential can be determined from the total charge density by solving Poisson's equation. The EFG can be directly computed from the charge density by using a method developed by Schwarz *et al.*[72] This approach is characterized by the component with the greatest modulus V_{zz} and the asymmetry parameter $\eta = \frac{V_{xx} - V_{yy}}{V_{zz}}$, where the principal components have been chosen in such a way that $|V_{zz}| > |V_{yy}| > |V_{xx}|$. V_{zz} can be written as

$$V_{zz} = 2\sqrt{\frac{4\pi}{5}} \int \frac{\rho(0)}{r^3} Y_{2,0}(\hat{r}) dr,$$

with the spherical harmonic $Y_{2,0}(\hat{r})$. Note that the spherically symmetric part of $\rho(r)$ does not contribute to the EFG.

The calculated EFG can be very sensitive to small changes in the charge distributions especially near the nucleus, hence, highly accurate calculations are needed. As the EFG reflects the asphericity of the charge-density distribution near the probe nucleus, it is directly related to the electron-density distribution, the nature of the chemical bond, and the symmetry in the nearest environment of the chemical bond. The EFG has three main contributions.[73] First, the asymmetric distribution of the valence electrons of the atom under consideration defined as

$$V_{zz,\mathrm{val}} = \left\langle \frac{\rho(3z^2 - r^2)}{r^5} \right\rangle.$$

Second, the lattice contribution arising from the charges in the surroundings of the Mössbauer atom (in a lattice of noncubic symmetry represented as the effect of the crystal "residue") (viz., parts of the structure outside the domain of the site under consideration). Third, the contribution from point charges Q_V and polarization of inner shells (core polarization). This contribution is a consequence of the influence of the two former effects on the core electrons, that are otherwise spherically symmetric and produce no EFG. This contribution is defined as

$$V_{zz,\mathrm{nucl}} = \sum_v \frac{Q_V(3z_v^2 - r_v^2)}{r_v^2},$$

where the summation is performed over the atoms of the lattice fragment considered.

The positive $V_{zz,\mathrm{val}}$ values at the Fe1^s site (Table IV) show that excess charges are accumulated in the xy plane and the contributions from $d_{x^2-y^2}$, d_{xy}, p_x, and p_y orbitals dominate over those of d_{z^2}, d_{xz}, d_{yz}, and p_z orbitals oriented along the z axis. This is associated with the oxygen vacancy at the apical site which alters both the charge density and (hence) the EFG. On the other hand, the negative contribution at Fe2^o reflects charge accumulation along the z axis as well as the strong covalent bonding between Fe2^o and the apical oxygen atoms. The covalence effect[74] which involves the Fe-3d and 4p-valence orbitals plays an important role for the size of EFG and Δ_Q. Note that the COHP analysis also identified Fe1^s-Ob as the stronger bonds around Fe1 while the strongest Fe2^o-O bonding interaction is perpendicular to the base of the octahedra, viz., the Fe2^o-Oa bonds (see Fig. 2).

Moreover, from Fig. 1(a), it is evident that the valence-charge density is relatively more spherical around Fe2^o than around Fe1^s. This indicates that the bonding between Fe2^o and O is more ionic than that between Fe1^s and O, viz., consistent with our finding that the formal Fe^{4+} resides at the Fe2^o site. In contrast, the charge density at the Fe2^o nuclear site [see the charge transfer plot in Fig. 1(b)] is more deformed than that around the Fe1^s site, as can be seen from the significant deviation from spherical symmetry (fourfold rotational symmetry) near the core of the Fe2^o site, viz., close to the Fe2^o nuclei. Although the Fe2^o-O bonds have a dominant ionic character, additional significant aspherical distortions occur very close to the Fe2^o nuclei. This results in a larger EFG for Fe2^o compared to that for Fe1^s (a considerable part of this anisotropy stems from a region very close to the nucleus and hence gets amplified by the factor $1/r^3$).

Let us further analyze EFG in more detail. EFG is more specifically determined by the $l=2$ components of the lm-projected charge density $\rho_{2m}(r)$. Such $l=2$ components arise from the anisotropy of the p- and d-charge densities, whereas s electrons do not contribute owing to their spherical symmetry and the mixed s-d and p-d terms are very small. To a good approximation, the EFG is therefore determined by the anisotropy of the local p and d charges,[75] viz.,

$$V_{zz} = a\Delta N_p + b\Delta N_d, \tag{3}$$

where ΔN_p and ΔN_d are the anisotropic p and d charges, which for the considered symmetry with the z axis oriented along [001] are given by

$$\Delta N_p = \int_0^{E_F} dE \left[\frac{1}{2}[n_{p_x}(E) + n_{p_y}(E)] - n_{p_z}(E) \right] \tag{4}$$

$$\Delta N_d = \int_0^{E_F} dE \left[n_{d_{x^2-y^2}}(E) + n_{d_{xy}}(E) - \frac{1}{2}[n_{d_{xz}}(E) + n_{d_{yz}}(E)] - n_{d_{z^2}}(E) \right]. \tag{5}$$

The calculated values of ΔN_p and ΔN_d for the Fe1^s site are $-0.0082e$ and $0.0094e$, respectively, and the corresponding values for the Fe2^o site are $0.0046e$ and $0.0346e$. The EFG at the Fe2^o site is more than three times larger than that at the Fe1^s site, as reasoned below. The Fe^{4+} ion in the high-spin state has a singly-occupied e_g orbital which is purely $Y_{2,0} \propto 3z^2 - 1$ (with respect to the crystallographic c axis). This orbital has the most distinct nonspherical character among

the *d* orbitals (see the orbital ordering scheme in Fig. 6 of Ref. 1) and this leads to large EFG.

In short, we have been able to reproduce the experimentally reported Δ_Q for both the $Fe1^s$ and $Fe2^o$ sites. The oxygen vacancies play an important role in determining the charge-density distribution at the $Fe1^s$ site. In particular, the redistribution of the electron density around the $Fe1^s$ nucleus changes Δ_Q from negative to positive. A more detailed analysis shows that Δ_Q does not depend on the total charge at each site but rather on the anisotropy in the charge distribution at the nucleus. Even if two sites have same total charges, the anisotropy in the charge distribution and hence Δ_Q can be different. It may be noted that for Fe^{3+} in a given structural framework, Δ_Q increases with increasing tetrahedral distortion.[76] For example, for the two different Sn sites in SnO with same valence state but different site symmetry [Δ_{IS} is equal whereas Δ_Q and EFG differ by a factor of 2 (Ref. 77)]. The Δ_Q is decided by the site symmetry of the atom, character of the electrons involved in the bonding interaction with the neighbors, coordination number, interatomic distance, etc. Therefore, the value of Δ_Q obtained from Mössbauer spectra is not appropriate for an unambiguous assignment of charge states.

VI. CONCLUSION

Bond length depends on coordination number and geometry, spin state, charge state, neighboring ions, bond character, size of the constituents of the compound, temperature, pressure, etc. Hence, the bond length alone cannot be used to characterize formal oxidation states for ions.

We have demonstrated that it is possible to evaluate the Mössbauer parameters hyperfine field, isomer shift, and quadrupole moment with reasonable accuracy using density-functional calculations. Using these findings, we have analyzed the origin of the Mössbauer parameters and established that the hyperfine field reflects the spin density at the Fe sites in $Sr_4Fe_4O_{11}$, whereas the oxidation state of an ion is decided by the total charge density at the site concerned. The spin density only provides information about the difference in charge density between the majority- and minority-spin channels, influenced by the exchange splitting and not by the valence state. The quadrupole splitting reflects the EFG which in turn reveals the asymmetry in the charge-density distribution at the nucleus. Ions with the same valence state can have different EFGs depending on the coordinating atoms, the character of electrons (*s*, *p*, or *d*), and the chemical bonding with the neighbors (directional or nondirectional bonding). The EFG does not provide information about the total charge at a site and hence not the valence state of its occupant. The isomer shift bestows the amount of the charge density at the probe nucleus and depends on the degree of localization or delocalization of charges. However, it does not provide information about the total charge at a given site. Moreover, even if two ions are in the same valence state, the degree of localization or delocalization may be different depending on the hybridization interaction with the neighbors (a short Fe-O distance will increase the delocalization and hence decrease the isomer shift), nature of the electrons (*s* electrons will be more spatially spread than *p* and *d* electrons), and especially how the electrons are distributed within the site (viz., if the same amount of electrons is distributed almost uniformly, then the isomer shift will be smaller, and in contrast, if the distribution is such that more electrons are at the nucleus and less in the outer region, then the isomer shift will be larger). So, the isomer shift reflects the shape of electron distribution and the degree of localization of the electrons but does not provide information about the total charge at a given site, and hence, the isomer shift is not decisive for establishing charge states.

For pure ionic materials, the evaluation of oxidation state from comparison of Mössbauer parameters with those of reference systems may work, although there is no direct correlation. The atom-specific nature of the Mössbauer measurements can be used to distinguish between ions with different oxidation states, spin density, asymmetry in charge distribution, degree of localization of electrons at different sites, etc. However, this approach cannot be used to quantify the actual charge states of the ions concerned. The hitherto assumed correlation between oxidation states and Mössbauer parameters does not have a proper physical basis and such deliberation should not be used alone to establish the oxidation state especially in a system with mixed ionocovalent bonding.

ACKNOWLEDGMENTS

The authors are grateful for the financial support from the Research Council of Norway. Parts of these calculations were carried out at the Norwegian supercomputer facilities. P.R. wishes to thank P. Dederichs (Forschungszentrum Jülich), H. Akai (Osaka University), and S. Blügel (Forschungszentrum Jülich) for useful discussions and P. Novák (Academy of Sciences of the Czech Republic) and S. Cottenier (Katholieke Universiteit Leuven) for helpful communications.

*ponniah.ravindran@kjemi.uio.no

[1] R. Vidya, P. Ravindran, H. Fjellvåg, and A. Kjekshus, Phys. Rev. B **74**, 054422 (2006).

[2] P. Ravindran, R. Vidya, H. Fjellvåg, and A. Kjekshus, Phys. Rev. B **77**, 136402 (2008).

[3] P. Adler, Phys. Rev. B **77**, 136401 (2008).

[4] J. P. Hodges, S. Short, J. D. Jorgensen, X. Xiong, B. Dabrowski, S. M. Mini, and C. W. Kimball, J. Solid State Chem. **151**, 190 (2000).

[5] M. Schmidt, M. Hofmann, and S. J. Campbell, J. Phys.: Condens. Matter **15**, 8691 (2003).

[6] Inorganic Crystal Structure Database (ICSD), Version 2007-02,

Karlsruhe, Germany, 2007.
[7] N. E. Brese and M. O'Keeffe, Acta Crystallogr., Sect. B: Struct. Sci. **47**, 192 (1991).
[8] T. Arima, D. Higashiyama, Y. Kaneko, J. P. He, T. Goto, S. Miyasaka, T. Kimura, K. Oikawa, T. Kamiyama, R. Kumai, and Y. Tokura, Phys. Rev. B **70**, 064426 (2004).
[9] N. L. Ross, J. Zhao, and R. J. Angel, J. Steroid Biochem. **177**, 3768 (2004).
[10] A. G. Tutov and V. N. Markin, Izv. Akad. Nauk SSSR, Neorg. Mater. **6**, 2014 (1970).
[11] H. Pinto, M. Melamud, and H. Shaker, Acta Crystallogr., Sect. A: Cryst. Phys., Diffr., Theor. Gen. Crystallogr. **A33**, 663 (1977).
[12] P. Enghag, *Encyclopedia of the Elements* (Wiley-VCH, Weinheim, 2004).
[13] T. Takeda, R. Kanno, Y. Kawamoto, M. Takano, S. Kawasaki, T. Kamiyama, and F. Izumi, Solid State Sci. **2**, 673 (2000).
[14] W. W. Malinovskii and H. Kedesdy, J. Am. Chem. Soc. **76**, 3090 (1954).
[15] W. B. Pearson, *The Crystal Chemistry and Physics of Metals and Alloys* (Wiley-Interscience, New York, 1972) p. 164.
[16] F. Bouree, J.-L. Baudour, E. Elbadraoui, J. Musso, C. Laurent, and A. Rousset, Angew. Chem., Int. Ed. Engl. **25**, 217 (1996).
[17] S. C. Abrahams, J. M. Reddy, and J. L. Bernstein, J. Chem. Phys. **42**, 3957 (1965).
[18] M. Penicaud, B. Siberchicot, C. B. Sommers, and J. Kübler, J. Magn. Magn. Mater. **103**, 212 (1992).
[19] J. Smit and H. P. Wijn, *Ferrites* (Philips, Eindhoven, 1959), p. 149.
[20] D. Levy, A. Pavesy, and M. Hanfland, Phys. Chem. Miner. **27**, 638 (2000).
[21] M. E. Fleet, Acta Crystallogr., Sect. B: Struct. Crystallogr. Cryst. Chem. **37**, 917 (1981).
[22] E. J. W. Verwey and J. H. De Boer, Recl. Trav. Chim. Pays-Bas **55**, 531 (1936).
[23] O. Eriksson, M. S. S. Brooks, and B. Johansson, Phys. Rev. B **41**, 7311 (1990).
[24] G. Kresse and J. Hafner, Phys. Rev. B **47**, 558 (1993); G. Kresse and J. Furthmuller, Comput. Mater. Sci. **6**, 15 (1996).
[25] P. E. Blöchl, Phys. Rev. B **50**, 17953 (1994).
[26] G. Kresse and D. Joubert, Phys. Rev. B **59**, 1758 (1999).
[27] W. Kohn and L. J. Sham, Phys. Rev. **140**, A1133 (1965).
[28] M. C. Payne, M. Teter, D. C. Allen, T. A. Arias, and J. D. Joannopoulos, Rev. Mod. Phys. **64**, 1045 (1992).
[29] P. Pulay, Chem. Phys. Lett. **73**, 393 (1980).
[30] A. Savin, R. Nesper, S. Wengert, and T. F. Fässler, Angew. Chem., Int. Ed. Engl. **36**, 1808 (1997).
[31] O. K. Andersen and O. Jepsen, Phys. Rev. Lett. **53**, 2571 (1984).
[32] R. Dronskowski and P. E. Blöchl, J. Phys. Chem. **92**, 5397 (1993).
[33] G. Krier, O. Jepsen, A. Burkhardt, and O. K. Andersen, Tight Binding LMTO-ASA Program Version 4.7, Stuttgart, Germany, 1999.
[34] H. Bilz and W. Kress, *Phonon Dispersion Relations in Insulators* (Springer, Berlin, 1979).
[35] M. Posternak, R. Resta, and A. Baldereschi, Phys. Rev. B **50**, 8911 (1994).
[36] W. Zhong, R. D. King-Smith, and D. Vanderbilt, Phys. Rev. Lett. **72**, 3618 (1994).
[37] Ph. Ghosez, X. Gonze, P. Lambin, and J. P. Michenaud, Phys. Rev. B **51**, 6765 (1995).
[38] R. M. Martin, Phys. Rev. B **9**, 1998 (1974).
[39] R. Pick, M. H. Cohen, and R. M. Martin, Phys. Rev. B **1**, 910 (1970).
[40] S. Blügel, H. Akai, R. Zeller, and P. H. Dederichs, Phys. Rev. B **35**, 3271 (1987).
[41] D. Torumba, V. Vanhoof, M. Rots, and S. Cottenier, Phys. Rev. B **74**, 014409 (2006).
[42] T. Kotani and H. Akai, J. Magn. Magn. Mater. **177-181**, 569 (1998).
[43] J. P. Perdew and A. Zunger, Phys. Rev. B **23**, 5048 (1981).
[44] H. Akai and T. Kotani, Hyperfine Interact. **120/121**, 3 (1999).
[45] H. Ebert, H. Winter, B. L. Gyorffy, D. D. Johnson, and F. J. Pinski, J. Phys. F: Met. Phys. **18**, 719 (1988).
[46] H. Ebert, H. Winter, D. D. Johnson, and F. J. Pinski, J. Phys.: Condens. Matter **2**, 443 (1990).
[47] H. Akai, M. Akai, S. Blügel, B. Drittler, H. Ebert, K. Terakura, R. Zeller, and P. H. Dederichs, Prog. Theor. Phys. Suppl. **101**, 11 (1990) and references therein.
[48] M. Elzain, A. La Rawas, Y. Yousif, A. Gismelseed, A. Rais, I. Al-Omari, K. Bouziane, and H. Widatallah, Hyperfine Interact. **156/157**, 205 (2004).
[49] Y. Kong, J. Peizl, and F. Li, J. Phys.: Condens. Matter **10**, 8341 (1998).
[50] R. Kirsch, M. J. Prandolini, O. Beutler, W. D. Brewer, M. Gauyters, J. Kapoor, D. Riegel, H. Ebert, and S. Frota-Pessoa, Europhys. Lett. **59**, 430 (2002).
[51] J. Klatyk, W. Schnelle, F. R. Wagner, R. Niewa, P. Novák, R. Kniep, M. Waldeck, V. Ksenofontov, and P. Gütlich, Phys. Rev. Lett. **88**, 207202 (2002).
[52] P. Ravindran, A. Kjekshus, H. Fjellvåg, P. James, L. Nordström, B. Johansson, and O. Eriksson, Phys. Rev. B **63**, 144409 (2001).
[53] D. Bonnenberg, K. A. Hempel, and H. P. Wijn, in *3d, 4d, and 5d Elements, Alloys, and Compounds*, Landolt-Börnstein, New Series, Group III, Vol. 19a, edited by H. P. Wijn (Springer, Berlin, 1986), p. 142.
[54] E. Makovicky, K. Forcher, W. Lottermoser, and G. Amthauer, Mineral. Petrol. **43**, 73 (1990).
[55] E. Simanek and Z. Sroubek, Phys. Rev. **163**, 275 (1967).
[56] W. Marshall, in *Proceedings of the Second International Conference on the Mössbauer Effect*, edited by A. H. Shoen and D. M. J. Compton (Wiley, New York, 1962), p. 263.
[57] K. K. Rao, M. C. W. Evans, R. Cammack, D. O. Hall, C. L. Thompson, P. J. Jackson, and C. E. Johnson, Biochem. J. **129**, 1063 (1972).
[58] G. Weyer, A. Nylandste-Larsen, B. I. Deutch, J. U. Andersen, and E. Antoncik, Hyperfine Interact. **1**, 93 (1975).
[59] M. Akasaka, Phys. Chem. Miner. **9**, 205 (1983).
[60] R. Ingalls, F. Van der Woude, and G. A. Sawatzky, in *Mössbauer Isomer Shifts*, edited by G. K. Shenoy and F. E. Wagner (North-Holland, Amsterdam, 1978), p. 361.
[61] H. Ohashi, J. Jpn. Assoc. Mineral. Petrol. Econ. Geol. **79**, 235 (1984).
[62] A. A. Temperley and H. W. Lefevre, J. Phys. Chem. Solids **27**, 85 (1966).
[63] R. L. Wappling, S. Haggstrom, S. Rundqvist, and J. Karlsson, J. Solid State Chem. **3**, 276 (1971).
[64] P. Ayyub, M. Multani, M. Barma, V. R. Palkar, and R. Vijayaraghavan, J. Phys. C **21**, 2229 (1988).
[65] J. A. Moyzis, G. Depasquali, and H. G. Drickamer, Phys. Rev.

172, 665 (1968).
[66] D. L. Williamson, in *Mössbauer Isomer Shifts*, edited by G. K. Shenoy and F. E. Wagner (North-Holland, Amsterdam, 1978), p. 317.
[67] J. E. Inglesfield, J. Phys. Chem. Solids **31**, 1435 (1970).
[68] A. Falepin, S. Cottenier, C. M. Comrie, and A. Vantomme, Phys. Rev. B **74**, 184108 (2006).
[69] W. J. Nickolson and G. Burns, Phys. Rev. **133**, A1568 (1964).
[70] N. N. Greewood and T. C. Gibb, *Mössbauer Spectroscopy* (Chapman and Hall, London, 1971).
[71] M. H. Cohen and F. Reif, Solid State Phys. **5**, 321 (1957).
[72] K. Schwarz, C. Ambrosch-Draxl, and P. Blaha, Phys. Rev. B **42**, 2051 (1990).
[73] *Mössbauer Spectroscopy*, edited by U. Gonser (Springer, Berlin, 1975); *Mössbauer Spectroscopy and Transition Metal Chemistry*, edited by P. Gütlich, R. Link, and A. Trautwein (Springer, Berlin, 1978).
[74] M. Braga, A. C. Pavano, and J. R. Leite, Phys. Rev. B **23**, 4328 (1981).
[75] P. Blaha, K. Schwarz, and P. H. Dederichs, Phys. Rev. B **37**, 2792 (1988); **38**, 9368 (1988).
[76] M. Akasaka and H. Ohashi, Phys. Chem. Miner. **12**, 13 (1985).
[77] A. Svane, N. E. Christensen, C. O. Rodriguez, and M. Methfessel, Phys. Rev. B **55**, 12572 (1997).